

Supporting Information

Room-Temperature Liquid Crystalline Unsymmetrical S-Annulated Perylene Diester Imide as a Dopant for Greenish-Yellow OLEDs with high EQE of 6.9 %

Paresh Kumar Behera,^a Sushanta Lenka,^b Feng Rong Chen,^b Mrinmoy Roy,^a Lu Chun-Chang,^c Chang-Hua Liu,^c Jwo-Huei Jou^{*b} and Ammathnadu Sudhakar Achalkumar^{*a,d}

*^aDepartment of Chemistry, Indian Institute of Technology Guwahati,
Guwahati, 781039, Assam, India.*

*^bDepartment of Materials Science and Engineering National Tsing Hua University 101,
Sec. 2, Kuang-Fu Road, Hsinchu 30013, Taiwan*

*^cInstitute of Photonics Technology, National Tsing Hua University 101, Sec. 2, Kuang-Fu Road, Hsinchu
30013, Taiwan*

*^dCentre for Sustainable Polymers, Indian Institute of Technology Guwahati,
Guwahati, 781039, Assam, India.*

Table of Contents

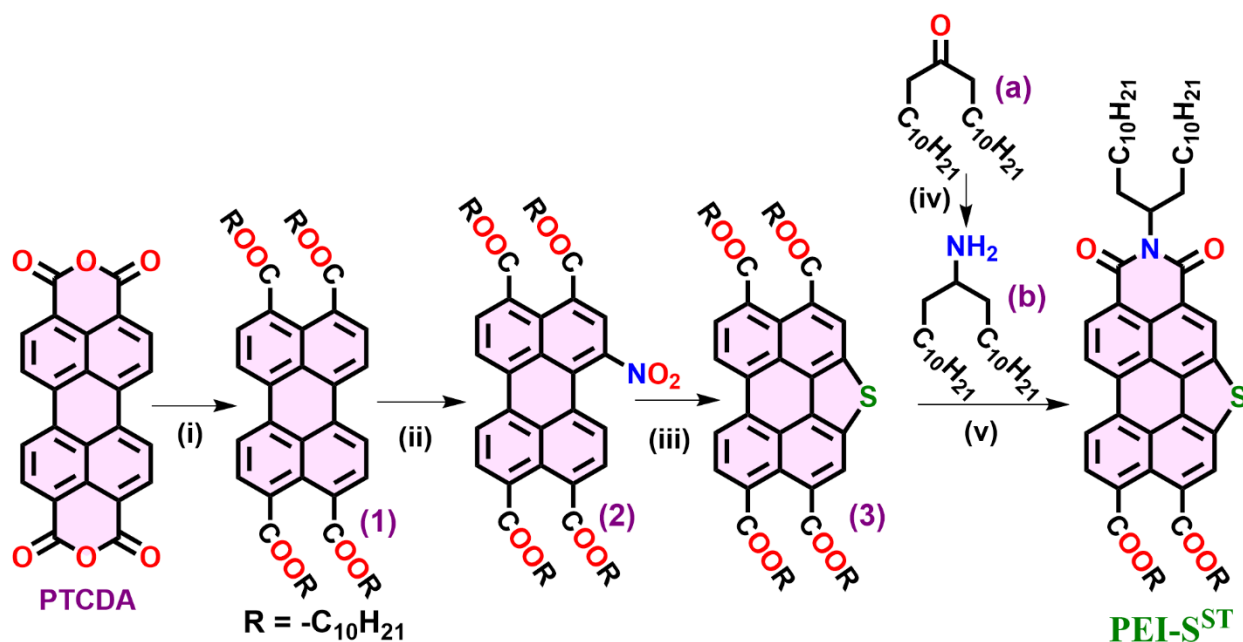
Serial Number	Contents	Page numbers
1	Materials and methods	S3
2	Experimental Section	S4-S5
3	NMR Spectra	S6
4	MALDI-TOF mass spectrometry	S7
5	Photophysical studies	S7-S8
6	Quantum yield measurement	S8-S9
7	Polarizing Optical Microscopy (POM)	S9
8	Differential Scanning Calorimetry (DSC)	S10
9	Thermogravimetric analysis (TGA)	S10
10	X-ray diffraction (XRD) studies	S11-S12
11	Cyclic Voltammetry	S13
12	Device Fabrication and characterization	S13-S15
13	DFT Studies	S16-S17
14	TD-DFT and NTO calculations	S17-S23
15	Electron-hole correlation plots for the individual states	S24-S25
16	Time resolved photoluminescence studies	S26
17	References	S26-S28

1. Materials and methods

Commercially available chemicals were utilized without further purification, and standard procedures were followed to dry the solvents. Chromatography was conducted using either silica gel (60-120 mesh) or neutral aluminum oxide. For thin-layer chromatography, aluminum sheets pre-coated with silica gel were employed. IR spectra were acquired at room temperature using a Perkin Elmer IR spectrometer (PerkinElmer UATR TWO). The spectral positions are reported in wave number (cm^{-1}) units. NMR spectra were recorded using a 600MHz Nuclear Magnetic Resonance (NMR) Spectrometer (Make: Bruker, Model: AVANCE III HD). Chemical shifts in ^1H NMR spectra were referenced to TMS as an internal standard and reported in ppm. Coupling constants were provided in Hz. Mass spectra were obtained using a MALDI-TOF mass spectrometer (Matrix Assisted Laser Desorption Ionization- Time of Flight, Make: BRUKER Model: AUTOFLEX SPEED) with α -Cyano-4-hydroxycinnamic acid as a matrix. The liquid crystalline behavior of the mesogenic compounds, including birefringence and fluidity, was investigated using a polarizing optical microscope (Nikon Eclipse LV100POL) equipped with a programmable hot stage (Mettler Toledo FP90). Observations were made with clean glass slides and coverslips. Differential scanning calorimetry (DSC) under a nitrogen atmosphere was used to determine transition temperatures and associated enthalpy changes. A Mettler Toledo DSC1 instrument was employed, and the peak temperatures corresponding to transitions obtained from DSC were consistent with the polarizing optical microscopic observations. The first heating and cooling cycles were conducted at a rate of $5\text{ }^{\circ}\text{C}/\text{min}$, and the transition temperatures were recorded. Variable temperature XRD studies were performed using samples filled in Lindemann capillaries. A high-resolution X-ray powder diffractometer (PANalytical X'Pert PRO) equipped with a high-resolution fast detector PIXCEL was used. The sample temperature was controlled using a Mettler hot stage/programmer (FP82HT/FP90). Thermogravimetric analysis (TGA) was carried out using a thermogravimetric analyzer (Mettler Toledo, model TG/SDTA 851 e) under a nitrogen flow at a heating rate of $10\text{ }^{\circ}\text{C}/\text{min}$. UV-Vis spectra were recorded using a Perkin-Elmer Lambda 750 UV/VIS/NIR spectrometer. Fluorescence emission in solution state was investigated using either a Horiba Fluoromax-4 fluorescence spectrophotometer or a Perkin Elmer LS 50B spectrometer. Cyclic Voltammetry (CV) studies were conducted using a Metrohm Autolab PGSTAT204 Electrochemical workstation with the assistance of NOVA software.

2. Experimental Section:

2.1. Synthetic Scheme



Reagents and conditions: (i) KOH, H₂O, 70 °C, 0.5 h, 1 M HCl, Aliquat 336, KI, 1-bromobutane, reflux, 12 h (76%); (ii) NaNO₂, HNO₃, 0 °C, 1 h (90%); (iii) Sulfur powder, anhyd NMP, N₂, 70 °C, 0.5 h, 180 °C, 12 h (74%); (iv) NH₄OAc, NaBH₃CN, MeOH, RT, 72 h (95%); (v) b, Zn(OAc)₂, imidazole, 150 °C, 25 min, 30W, 100 psi, MW (51%).

Compounds 1,^[S1] 2, 3,^[S1] were prepared as reported earlier.

2.2 Synthetic Procedure

2.2.1 Synthetic route of Tricosan-12-amine (b):

A 250 mL round-bottom flask was charged with 12-tricosanone (a) (5 g, 14.76 mmol), NH₄OAc (11.35 g, 147.6 mmol), NaBH₃CN (1.275 g, 1.38 mmol) and MeOH (100 mL) and stirred at room temperature (r.t.) for 72 h until the starting material was consumed (monitored by TLC). The reaction was quenched by drop wise addition of conc. HCl (~12 mL) and the solvents were removed by rotary evaporation. The resulting white solid was dissolved in H₂O (200 mL) and adjusted to pH ~10 with KOH, then extracted with CHCl₃ (3 × 150 mL) to give the desired product as a white solid (4.8g, 95.6%). ¹H-NMR (600MHz, CDCl₃): δ = 0.88 (t, 6H), 1.10-1.50 (m, 42H), 2.68 ppm (s, 1H).

2.2.2 General procedure for synthesis of PEI-SST:

Compound **3** (1 eq.), tricosan-12-amine (1.1 eq.), zinc acetate (1 eq.) and imidazole (1 g) were taken in a microwave vessel, flushed with nitrogen and placed in a microwave reactor. The mixture was heated to 150 °C for 30 minutes at 35 W and 100 psi pressure. After cooling, the reaction mixture was poured into a 2N HCl (10 mL) solution and extracted with chloroform. Organic layer was washed with water and saturated sodium chloride solution. The crude compound was purified by column chromatography on neutral alumina using 5% chloroform-hexane system. Further purification was done by repeated recrystallization from THF-methanol system.

PEI-SST: $R_f = 0.5$ (10% CHCl₃-Hexane); Bright Orange sticky solid, yield: 51 %; IR ν_{\max} in cm⁻¹: 2919, 2849, 1696, 1642, 1554, 1466, 1425, 1367, 1309, 1166, 1113, 1076, 1039, 953, 749, 722; ¹H NMR (600 MHz, CDCl₃, ppm): δ 9.06 (d, $J = 30$ Hz, 1H, H_{Ar}), 8.69 (dd, $J_1, J_2 = 6$ Hz, 1H, H_{Ar}), 8.60 (s, 1H, H_{Ar}), 8.58 (d, $J = 6$ Hz, 1H, H_{Ar}), 8.52 (d, $J = 6$ Hz, 1H, H_{Ar}), 8.31 (d, $J = 6$ Hz, 1H, H_{Ar}), 5.30 (m, 1H, NCH), 4.47- 4.44 (m, 4H, 2 \times -OCH₂), 2.35-2.33 (m, 2H), 1.95 (m, 2H), 1.91-1.87 (m, 4H), 1.52 (m, 4H), 1.42-1.18 (m, 60H), 0.87 (t, $J = 6$ Hz, 6H, 2 \times CH₃), 0.81 (t, $J = 6$ Hz, 6H, 2 \times CH₃). ¹³C NMR (150 MHz, CDCl₃): δ 168.26, 168.20, 165.10, 164.75, 163.97, 163.73, 137.08, 135.31, 132.86, 132.77, 131.06, 130.99, 130.73, 129.58, 129.16, 128.85, 127.15, 126.37, 125.81, 125.48, 125.35, 125.22, 122.55, 121.84, 121.58, 121.54, 121.09, 120.83, 66.22, 66.09, 54.79, 32.56, 31.95, 31.94, 31.89, 29.72, 29.68, 29.67, 29.65, 29.63, 29.49, 29.47, 29.39, 29.38, 29.33, 28.78, 28.74, 27.29, 26.17, 26.15, 22.70, 22.65, 14.12, 14.07. MALDI-TOF exact mass calculated for C₆₇H₉₆NO₆S(M+H)⁺: 1042.696, found: 1042.248.

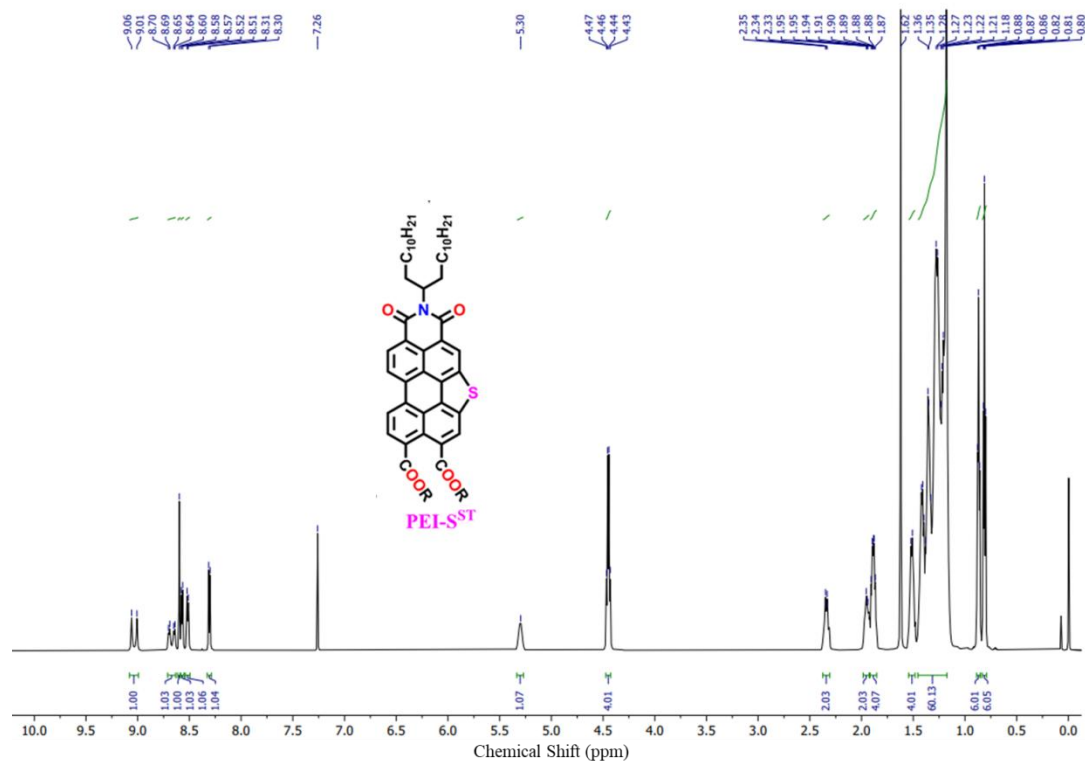


Figure S1. ^1H NMR (600 MHz) spectra of **PEI-SST** in CDCl_3 .

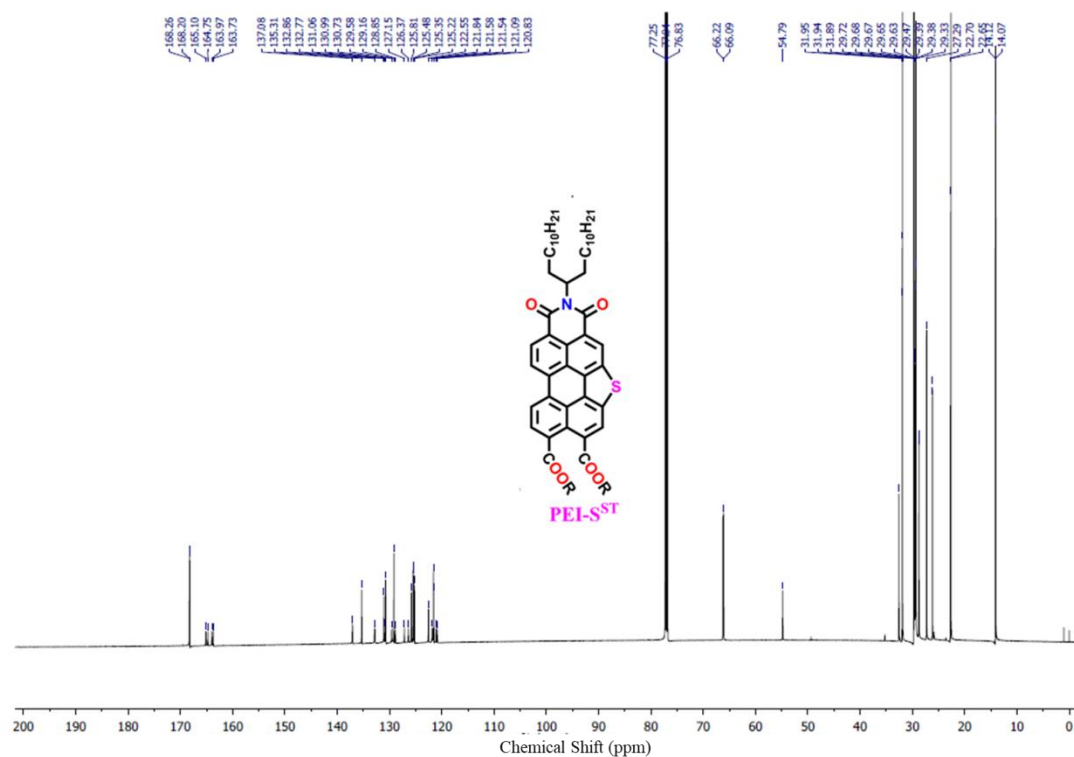


Figure S2. ^{13}C NMR (150 MHz) spectra of **PEI-SST** in CDCl_3 .

4. MALDI-TOF mass spectrometry

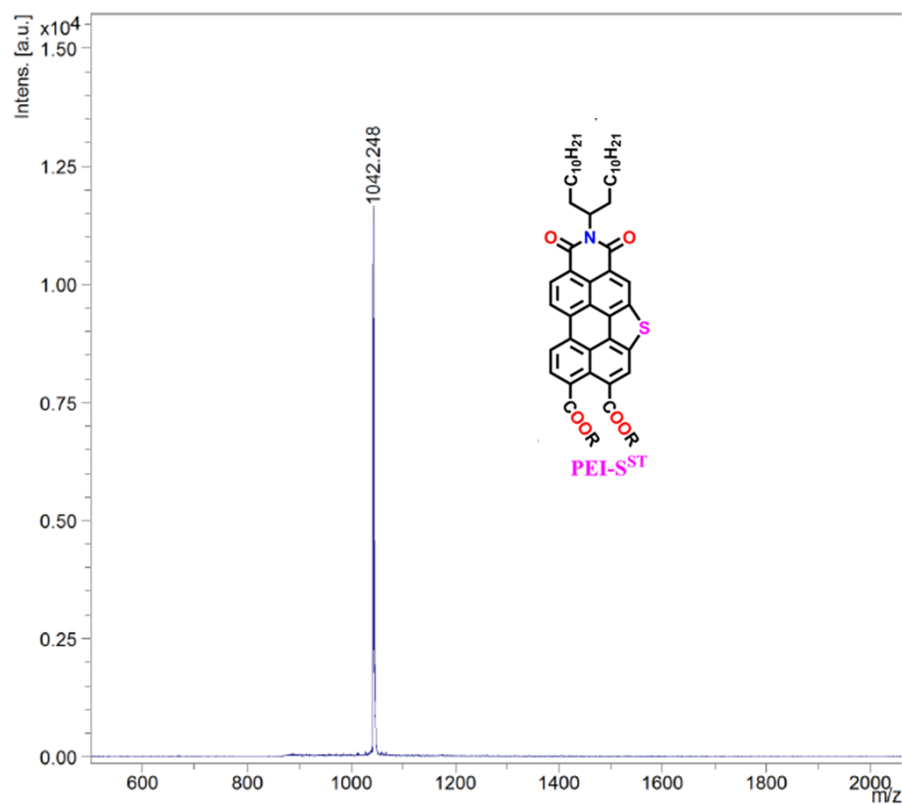


Figure S3. MALDI-TOF mass spectrum of **PEI-SST**.

5. Photophysical studies

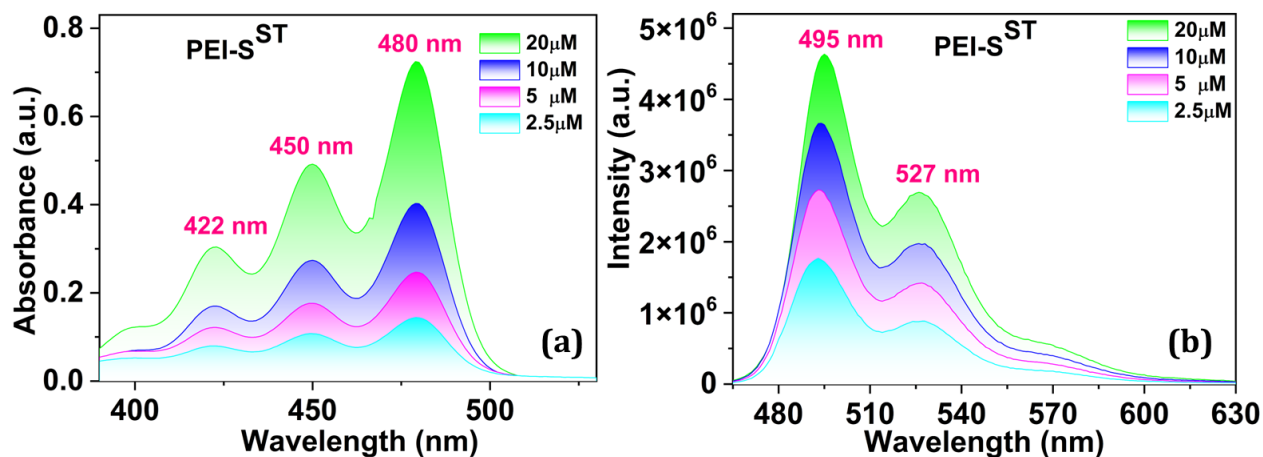


Figure S4. Absorption (a) emission (b) spectra of **PEI-SST** in chloroform solution as a function of concentration.

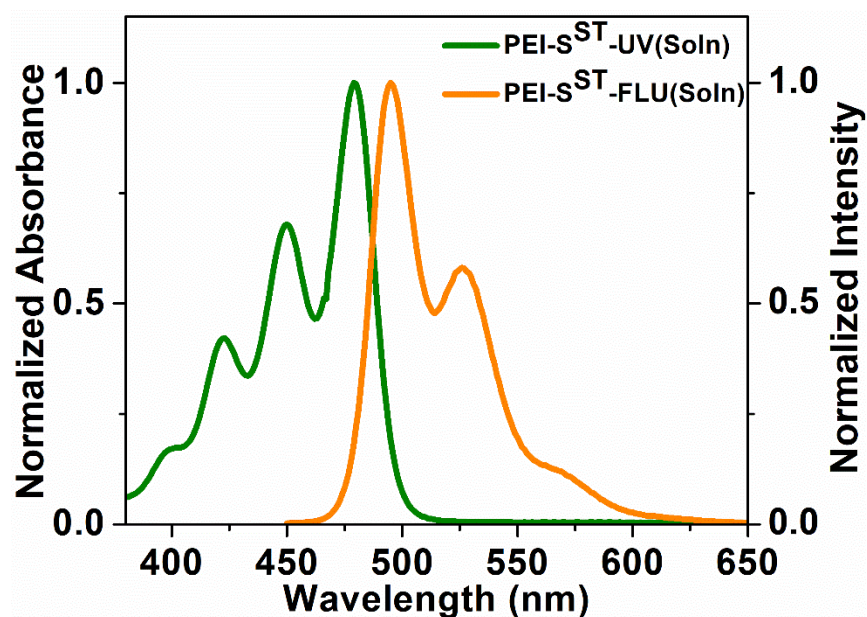


Figure S5. Overlay of absorption and emission spectra of **PEI-SST** in chloroform solution.

Table S1. Photophysical properties of **PEI-SST** in solution^a and thin film^b state.

Entry	Absorption [nm]	Emission ^c [nm]	Stokes Shift (cm ⁻¹)	Molar extinction coefficient (ε) (L mol ⁻¹ cm ⁻¹)	Quantum yield ^d (Q _s)	ΔE _{g, opt} ^e [eV]	Absorption [nm]	Emission ^f [nm]	Stokes Shift (cm ⁻¹)
PEI-SST	399, 422, 450, 480	495, 527	631	40,422	0.83	2.48	449, 507	593	5408

^aMicromolar solutions in CHCl₃. ^bPrepared by drop casting of millimolar solution in toluene. ^c The excitation wavelength λ_{ex} = 480 nm **PEI-SST**. ^d Relative quantum yields are calculated with respect to Rhodamine-6G (λ_{ex} = 530 nm) in ethanol solution as the standard and compounds in CHCl₃. ^e Calculated from the red edge of the absorption band. ^f Excited at the absorption maxima.

6. Quantum yield measurement (Relative)

Quantum yield was measured according to established procedure by using rhodamine 6g in ethanol as the standard. Absolute values were calculated according to the following equation:

$$Q_S = Q_R \times (m_S / m_R) \times (n_S / n_R)^2,$$

Where, Q: Quantum yield, m: Slope of the plot of integrated fluorescence intensity vs absorbance (Calculated from Fig.S15), n: refractive index (1.361 for ethanol and 1.445 for chloroform). The subscript R refers to the reference fluorophore i.e. rhodamine 6G solution in EtOH and subscript S refers to the sample under investigation. In order to minimize re-absorption effects, absorbance was kept below 0.15 at the excitation wavelength of 480 nm for compound **PEI-SST**. Quantum yield of rhodamine 6g in EtOH is 0.95. Simplified equation for the calculation after substituting the appropriate values is given below and values obtained are given in table below.

$$Q_S = 0.95 \times (m_S / m_R) \times (1.445/1.361)^2$$

Compounds	m_S	m_R	$Q_S^{a,b,c}$
PEI-SST	6.81784×10^8	8.63560×10^8	0.83

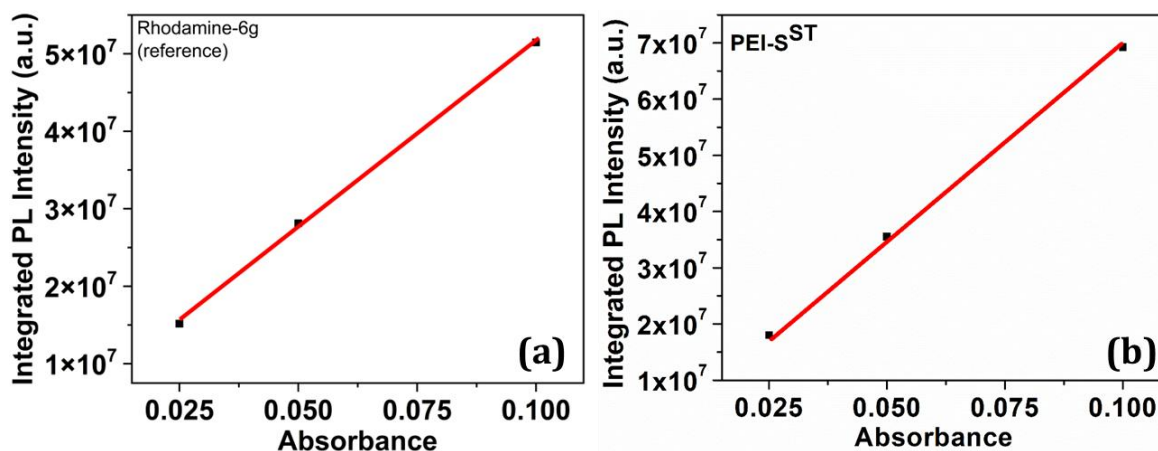


Figure S6. Plot of integrated photoluminescence intensity vs absorbance of reference rhodamine 6G (a) and compound **PEI-SST**(b).

7. Polarizing Optical Microscopy (POM)

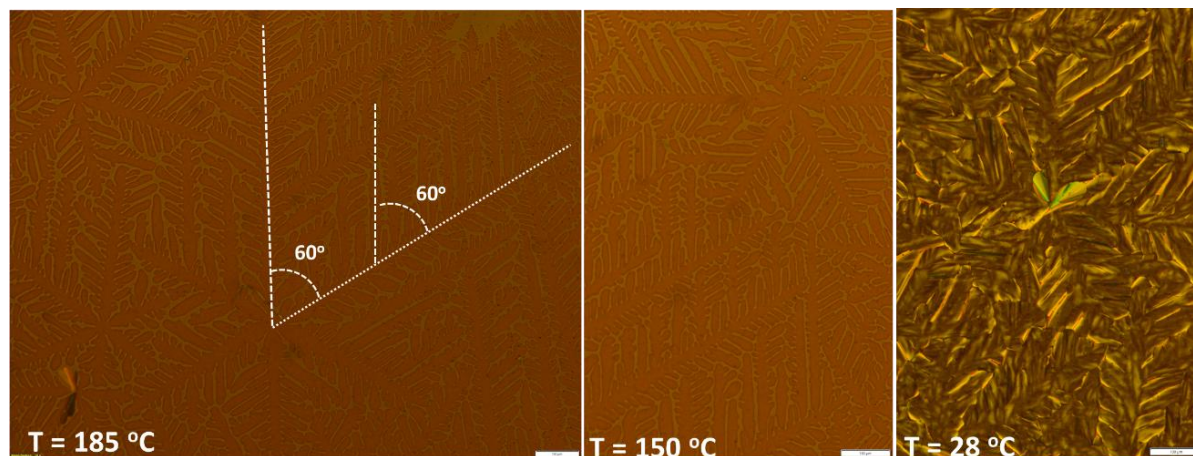


Figure S7. POM images obtained **PEI-SST** at different temperatures (scale bar 100 μm).

8. Differential Scanning Calorimetry (DSC)

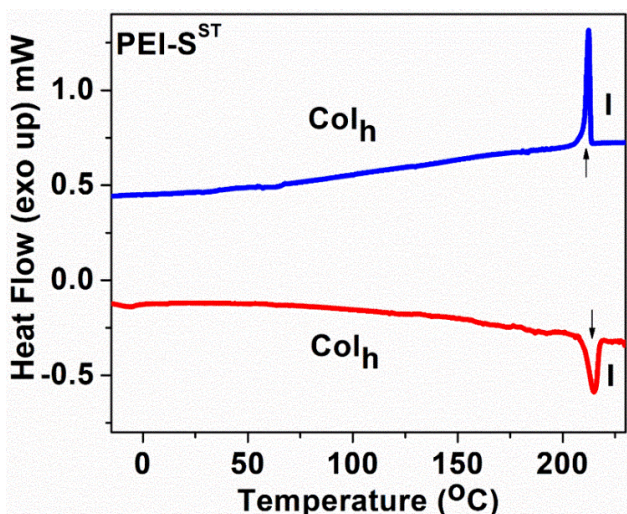


Figure S8. DSC thermograms of **PEI-SST** carried out at a rate of 5°C/min (red trace: second heating, blue trace: first cooling).

Table S2. Phase transition temperatures (°C), corresponding enthalpies (kJmol⁻¹)^a and decomposition temperatures^b of **PEI-SST** obtained from DSC^a and TGA^b.

Entry	Phase Sequence (kJ/mol)		T ₅ ^b (°C)
	Second heating	First Cooling	
PEI-SST	Col _h 216 (4.72) I	I 212 (4.48) Col _h	366
^a Peak temperatures in the DSC thermograms obtained during the second heating and first cooling cycles at 5 °C min ⁻¹ Col _h = Columnar hexagonal phase; I = Isotropic phase; ^b Temperature at which 5 weight % decomposition occurs as noted from TGA.			

9. Thermogravimetric analysis (TGA)

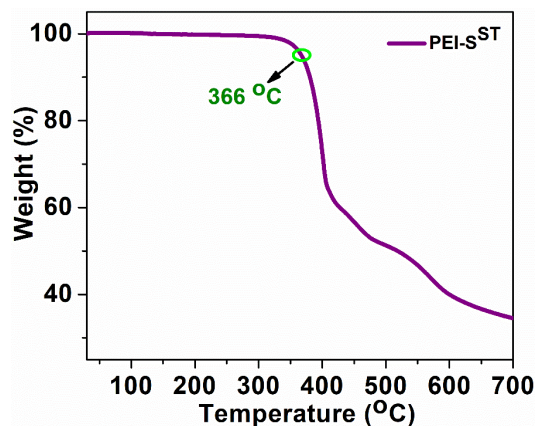


Figure S9. TGA plots of compound **PEI-SST** (heating rate of 10 °C/min, Nitrogen atmosphere).

10. X-ray diffraction studies (XRD)

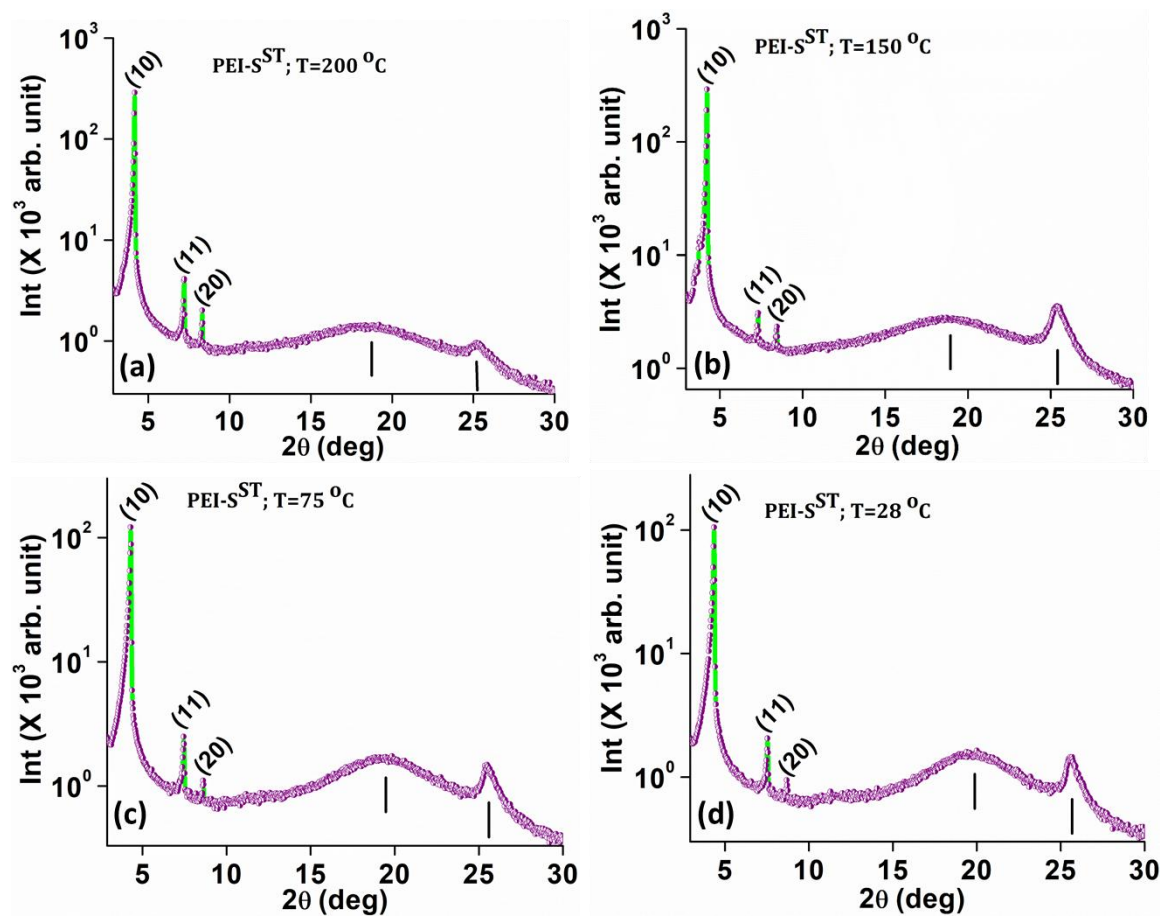


Figure S10. Plot of the intensity against 2θ obtained from the powder XRD pattern of the Col_h phases **PEI-SST** at different temperature intervals.

Table S3. Results of (*hkl*) indexation of XRD profiles of the compounds at a given temperature (T) of mesophases.^a

Compounds (D/Å)	Phase (T/°C)	d_{obs} (Å)	d_{cal} (Å)	Miller indices <i>hkl</i>	Lattice parameters (Å), Lattice area S (Å ²), Molecular volume (Å ³)
PEI-SST (35.5 Å) MW: 1042.7	Col _h (200)	20.89 12.05 10.45 4.73(h_a) 3.51(h_c)	20.96 12.26 10.55	100 110 200	$a = 24.20$ $S = 507.16$ $V = 1780.14$ $Z \approx 1$
	Col _h (150)	20.89 12.05 10.45 4.74(h_a) 3.50(h_c)	20.89 12.06 10.45	100 110 200	$a = 24.10$ $S = 503.27$ $V = 1761.46$ $Z \approx 1$
	Col _h (75)	20.49 11.85 10.25 4.59(h_a) 3.49(h_c)	20.49 11.83 10.25	100 110 200	$a = 23.64$ $S = 484.18$ $V = 1689.81$ $Z \approx 1$
	Col _h (28)	20.27 11.71 10.16 4.43(h_a) 3.48(h_c)	20.27 11.70 10.14	100 110 200	$a = 23.41$ $S = 475.61$ $V = 1651.64$ $Z \approx 1$
^a The diameter (D) of the disk (estimated from Chem 3D Pro 8.0 molecular model software from Cambridge Soft). d_{obs} : spacing observed; d_{cal} : spacing calculated (deduced from the lattice parameters; a for Col _h phase; c is height of the unit cell). The spacings marked h_a and h_c correspond to diffuse reflections in the wide-angle region arising from correlations between the alkyl chains and core regions, respectively.					

11. Cyclic Voltammetry

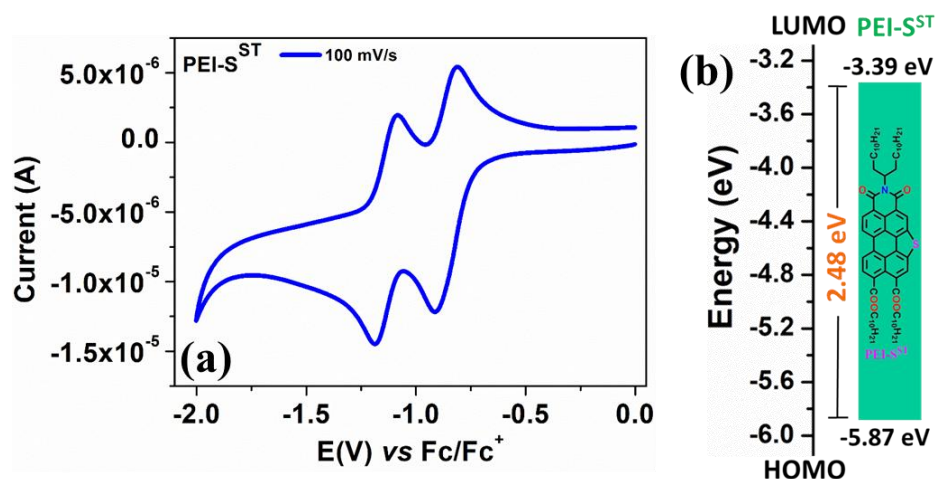


Figure S11. Cyclic voltammograms of **PEI-SST**(a); Energy band level diagram showing HOMO and LUMO energy levels.

Table S4. Electrochemical^{a,b} data and data obtained from DFT^h calculations for **PEI-SST**.

Electrochemical data					Data from DFT calculations		
Entry	E _{1st red} ^[c]	E _{LUMO} ^[d,e]	E _{HOMO} ^[d,f]	ΔE _{g,opt} ^[d,g]	E _{LUMO} ^[d,h]	E _{HOMO} ^[d,h]	ΔE _g ^[d,h]
PEI-SST	-0.91	-3.39	-5.87	2.48	-3.05	-5.87	2.82

^[a] 0.5 mM Dichloromethane solutions; ^[b] experimental conditions: Ag/AgNO₃ as reference electrode, glassy carbon working electrode, platinum wire counter electrode, TBAP (0.1M) as a supporting electrolyte, room temperature; ^[c] in volts (V); ^[d] in eV; ^[e] estimated from the formula by using E_{LUMO} = -(4.8 - E_{1/2, Fc/Fc⁺} + E_{red, onset}) eV; ^[f] estimated from the formula E_{HOMO} = (E_{LUMO} - E_{g,opt}) eV; E_{1/2, Fc/Fc⁺} = 0.50 V. ^[g] calculated from the red edge of the absorption band of each compound. ^[h] Obtained from DFT calculations by employing the combination of Becke3-Lee-Yang-Parr (B3LYP) hybrid functional and 6-31G(d,p) basis set using the Gaussian 09 package.

12. Device fabrication and characterization

Based on superior photophysical and electrochemical properties, the electroluminescent properties of **PEI-SST** emitter material was investigated. Multi-layered solution processed OLED was fabricated consisting of following device configurations: anode: ITO (125 nm)/HIL: PEDOT:PSS (40 nm)/ EML (20 nm)/ ETL: TPBi (35 nm)/EIL: LiF (1 nm)/cathode: Al (100 nm). Initially, ITO-coated glass substrates were cleaned to remove the greasy layer. The cleaning process was carried out with soap-solution, deionized water, acetone, and alcohol in a water-bath sonicator at an optimized time. Cleaned substrates were kept in an ultra-violet ozone system to expose them to UV light to remove residual solvents and further impurities. Then, these substrates were transferred into a nitrogen-purged glovebox for further processing of layers. Simultaneously, CBP as host and newly synthesized emitter (**PEI-SST**) for the emissive solution layer was dispersed into suitable solvents with a water-bath sonicator. Prepared solution was filtered with 0.45 μm

PTFE filters and mixed in desired ratio to prepare emissive layer. First, a hole-injection layer was prepared by spin-coating an aqueous solution of PEDOT: PSS at 4,000 rpm for 20 s. Subsequently, these substrates were annealed at 130 °C for 15 minutes. After cooled down the substrates, neat solution or emissive layer solution was spin-coated onto hole-injection layer at 2,500 rpm for 20 s. Then, these substrates were transferred into thermal evaporator to deposit subsequent layers. Then, TPBi was deposited as an electron-transport layer followed by the deposition of 0.5 nm LiF as an electron-injection layer and 100 nm Al as a cathode. All the layers of TPBi, LiF and Al were deposited subsequently via thermal evaporation method at base pressure of 4.0×10^{-6} Torr. After that, Fabricated devices were kept in the mini vacuum chamber during testing process and then measured at room temperature conditions. To analyse the device, the electroluminescence (EL) spectrum, luminance, and the CIE coordinates were obtained using a photo research (PR-655) spectrometer. The current density-voltage-luminance (J-V-L) characteristics were obtained by a computer mounted voltmeter (Keithley 2400) and spectrophotometer CS-100 Minolta.

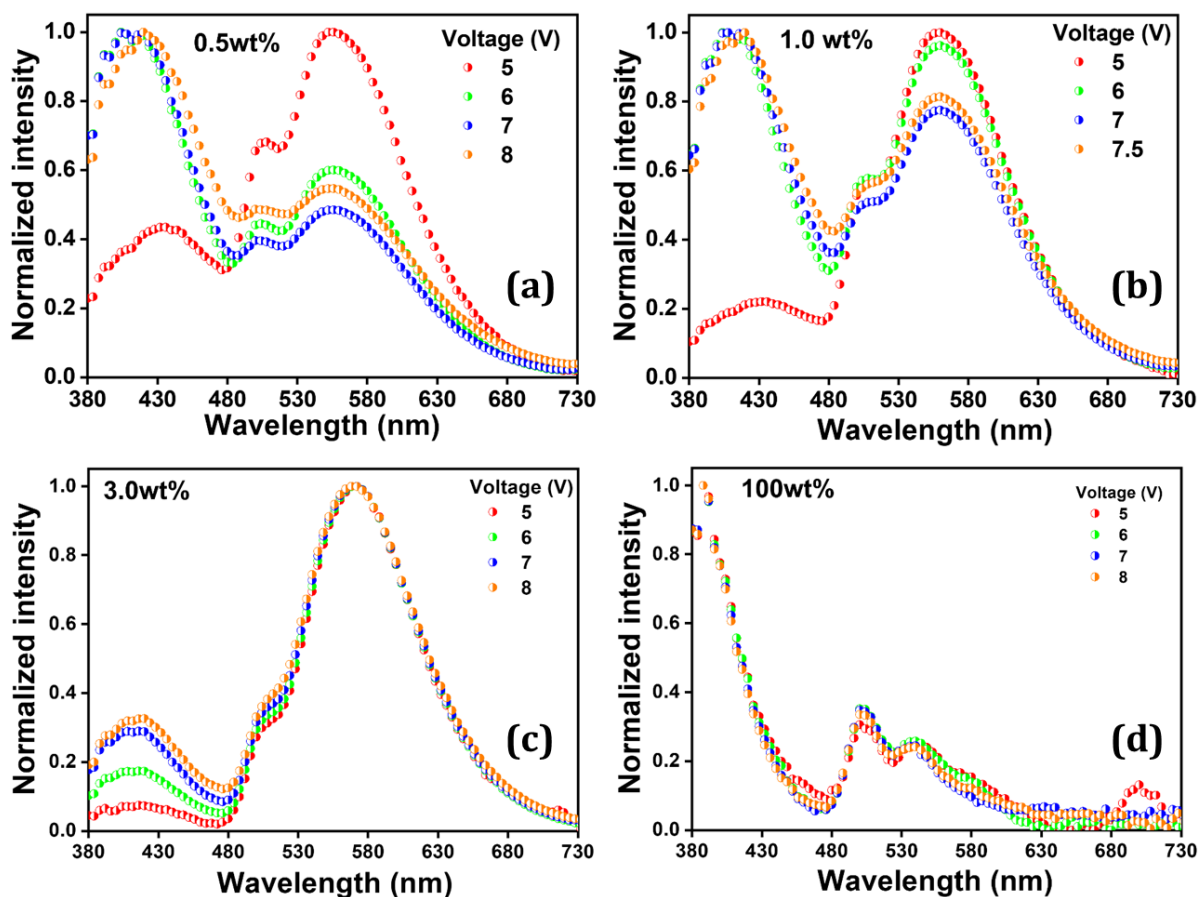


Figure S12. The electroluminescent spectra of **PEI-SST** at a varying voltage of the doped devices at varying concentrations (a) 0.5, (b) 1.0 and (c) 3.0 wt.% in the CBP host matrix, along with the (d) undoped (100 wt.%) device.

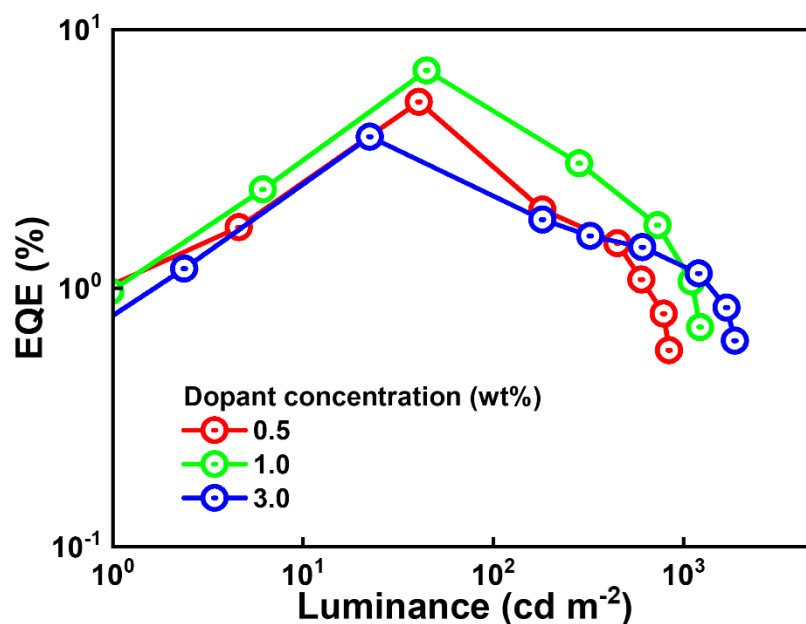


Figure S13. Electroluminescent properties of the OLED devices based on **PEI-SST** emitter doped in CBP host matrix showing EQE vs luminance characteristics.

Table S5. A comprehensive list of the driving voltage, power efficacy, current efficacy, external quantum efficiency (EQE), CIE coordinates, and luminance of the OLED device based on **PEI-SST** emitter doped in the CBP host matrix.

PEI-S ST (wt.%)	Driving Voltage (V)	Power efficacy (lm/W)	Current efficacy (cd/A)	EQE (%)	CIE (x, y)	Maximum luminance (cd/m ²)
		@ 100/1,000 cd/m ² and max			@ 100/1,000cd/m ²	
0.5	4.5	3.2/ -/ 4.3	5.7/ -/ 7.5	4.0/ -/ 5.3	(0.31, 0.34)/ -	1,609
1.0	4.5	5.3/ 1.2/ 6.0	9.3/ 2.6/ 10.6	6.2/ 1.3/ 6.9	(0.35, 0.42)/ (0.31, 0.33)	2,529
3.0	4.3	4.1/ 2.6/ 4.3	6.9/ 5.1/ 7.3	1.9/ 2.5/3.9	(0.41, 0.49)/ (0.39, 0.44)	2,933
100	5.6	- / - / -	- / - / -	- / - / -	- / - / -	6

13. DFT Studies

To understand the electronic properties and frontier molecular orbital energy level of compounds **PEI-SST** computational studies was carried out in B3LYP/6-31g(d,p) method using Gaussian 09 program package.^{S5} The absence of imaginary frequency ensured the energy minimized structure of all the compounds.

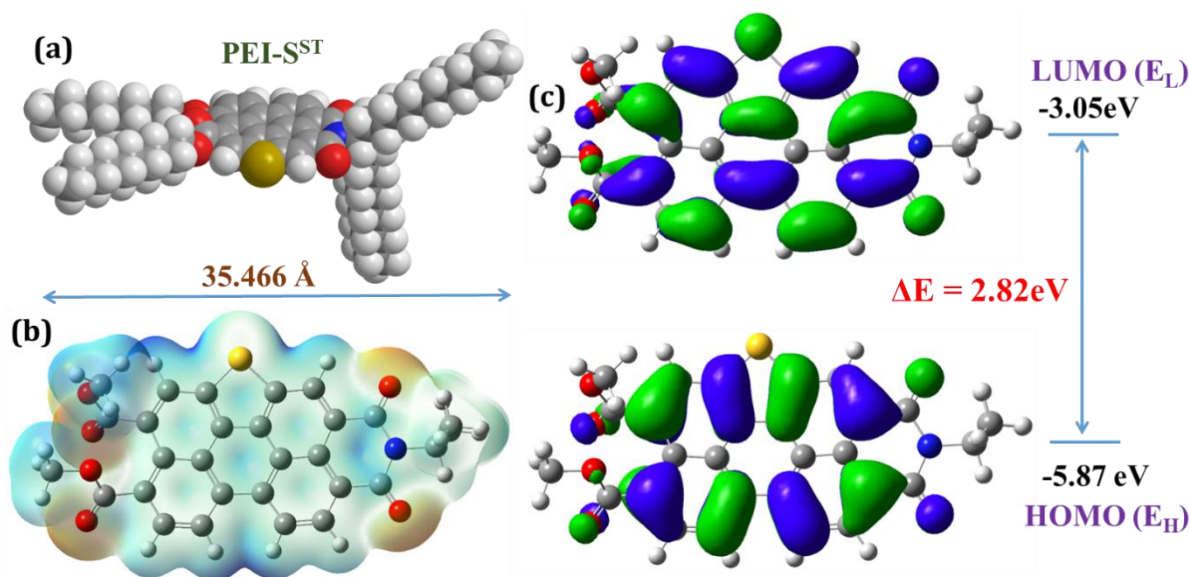


Figure S14. (a) Optimised geometry of **PEI-SST**; (b) 3D molecular electrostatic potential contour map of optimized structure of **PEI-SST** (In the mapped electro-static potential surface, the red and blue colors refer to the electron-rich and electron-poor regions, respectively, whereas the green color signifies the zero electrostatic potential, chain length is limited to methyl for clarity purpose); (c) Frontier molecular orbitals of **PEI-SST**, E_H and E_L denote energies of the highest occupied molecular orbital (HOMO) and the lowest unoccupied molecular orbital (LUMO), respectively.

DFT calculation data for **PEI-SST**:

Center Number	Atomic Number	Atomic Type	Coordinates (Angstroms)		
			X	Y	Z
1	6	0	-2.696925	2.675502	-0.231125
2	6	0	-1.357904	2.775655	-0.288683
3	6	0	-0.565572	1.689795	-0.220939
4	6	0	-1.247120	0.532753	-0.091024
5	6	0	-2.583111	0.374531	-0.029791
6	6	0	-3.327096	1.490771	-0.102387
7	6	0	-0.522665	-0.577160	-0.019811
8	6	0	-0.977438	-1.820497	0.097728
9	6	0	-2.308996	-1.959249	0.160839
10	6	0	-3.108717	-0.865134	0.098821
11	6	0	0.796640	1.690832	-0.259524
12	6	0	1.517890	0.547683	-0.194736

13	6	0	0.795848	-0.563167	-0.076764
14	6	0	1.544976	2.799527	-0.370261
15	6	0	2.876666	2.735116	-0.232840
16	6	0	3.547801	1.575756	-0.058141
17	6	0	2.865970	0.406276	-0.219519
18	6	0	3.351105	-0.866891	-0.382718
19	6	0	2.553894	-1.950521	-0.218271
20	6	0	1.240246	-1.811490	-0.012861
21	6	0	-4.462901	-1.014526	0.161727
22	7	0	-5.229513	0.144446	0.079549
23	6	0	-4.686064	1.421583	-0.047617
24	8	0	-5.377932	2.416371	-0.106958
25	8	0	-4.978479	-2.104758	0.282681
26	6	0	-6.706570	0.008523	0.134382
27	6	0	-7.296315	-0.768280	-1.058523
28	6	0	-7.221456	-0.503729	1.492819
29	16	0	0.139250	-2.784273	0.127827
30	6	0	4.864567	1.675764	0.337469
31	8	0	5.424380	2.755983	0.393954
32	8	0	5.554621	0.597744	0.854705
33	6	0	6.672639	0.833218	1.677692
34	6	0	4.630434	-1.118953	-0.823365
35	8	0	5.146659	-0.225649	-1.477364
36	8	0	5.338117	-2.302083	-0.797051
37	6	0	5.189107	-3.230842	0.253059
38	1	0	-3.259150	3.622834	-0.294892
39	1	0	-0.950044	3.792753	-0.392050
40	1	0	-2.707936	-2.982280	0.259521
41	1	0	1.102780	3.804114	-0.453205
42	1	0	3.366081	3.722609	-0.179964
43	1	0	2.896772	-2.982262	-0.369628
44	1	0	-7.197742	1.009110	0.041065
45	1	0	-8.407828	-0.689763	-1.078672
46	1	0	-6.914436	-0.358432	-2.021908
47	1	0	-7.063545	-1.854105	-1.038849
48	1	0	-8.331938	-0.431793	1.554320
49	1	0	-6.799818	0.103108	2.327045
50	1	0	-6.966175	-1.567045	1.688244
51	1	0	7.514718	1.239301	1.073706
52	1	0	6.401954	1.519555	2.510903
53	1	0	6.987344	-0.142946	2.110540
54	1	0	6.208020	-3.544974	0.574024
55	1	0	4.698057	-2.774077	1.139628
56	1	0	4.668957	-4.146381	-0.105456

14. TD-DFT and NTO calculations:

To understand the underlying mechanism behind the higher EQE observed with CBP hosted **PEI-SST**, excited states were calculated by time-dependent DFT (TD-DFT) calculations by using the ground state optimized geometries. Various mechanisms such as TADF,^{S3-S5} TTA,^{S6} and HLCT^{S7-}

^{S13} have been responsible to surpass this intrinsic limit in organic molecules where the triplet excitons can be harvested. Time-dependent DFT (TD-DFT) calculation using CAM-B3LYP/6-31G(d,p) level of theory was carried out to understand the excited state properties of the first 10 singlet (S_0 to S_{10}) and triplet states (T_1 to T_{10}) (Table S4). The energy difference between the high-lying singlet state S_1 and the triplet state T_4 was determined to be 0.004 eV (Fig. S17b). Natural Transition Orbitals (NTOs) were then generated and analyzed. Because of the similarity in energies of S_1 and T_4 , their NTOs were compared. Both the hole and particle of S_1 and T_4 are localized in the perylene core, indicating the prevalence of Local Excitation (LE) and confirming the presence of LE states. These LE states are crucial in providing the fluorescent emitter with a high quantum yield. Furthermore, the presence of states where the holes and particles are in different fragments indicates Charge Transfer (CT) excited states (Table S4). As a result, the excited states S_1 and T_3 exhibited Hybrid Local and Charge Transfer (HLCT) characteristics, primarily dominated by LE character with a lesser presence of CT character (Fig. S17a).

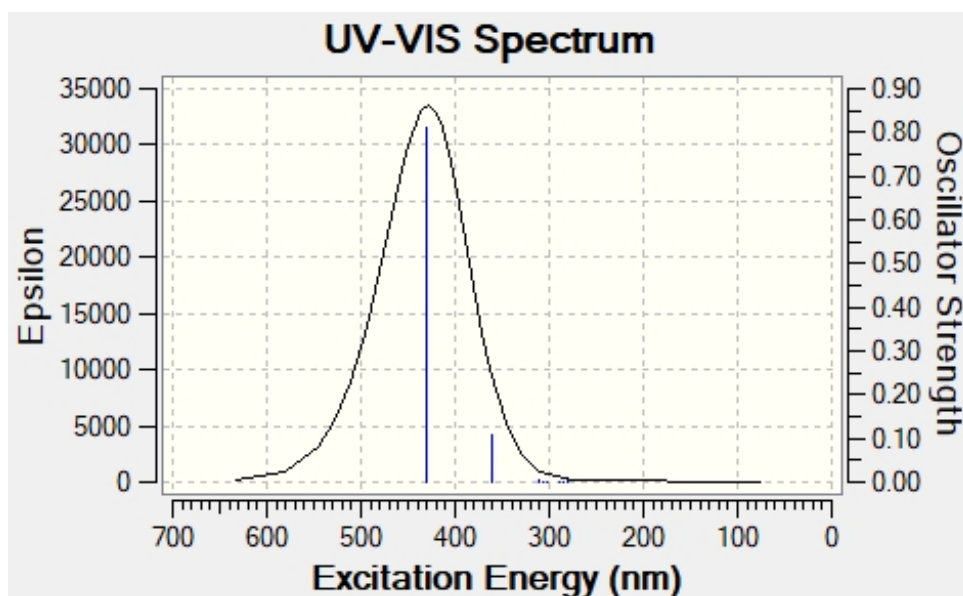
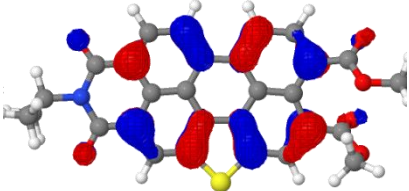
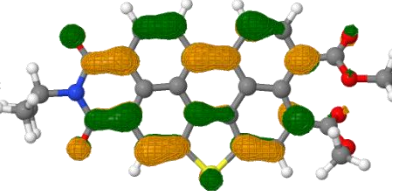
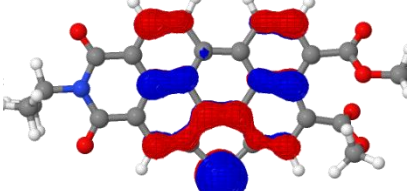
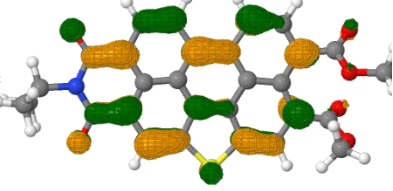
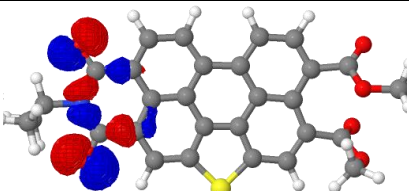
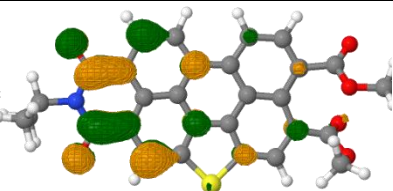
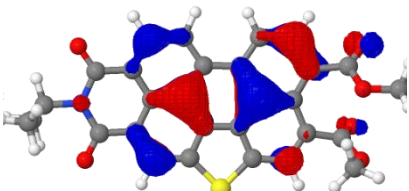
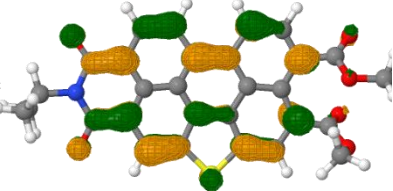
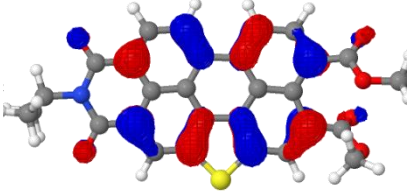
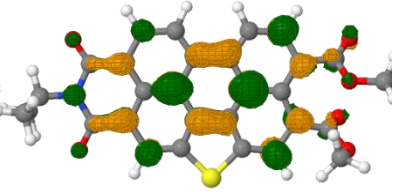
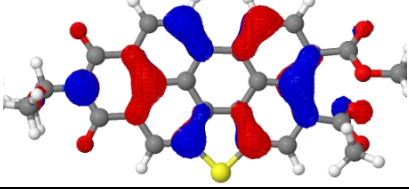
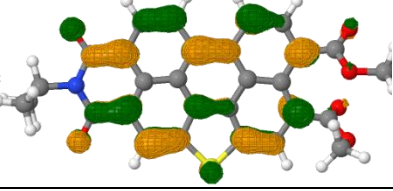
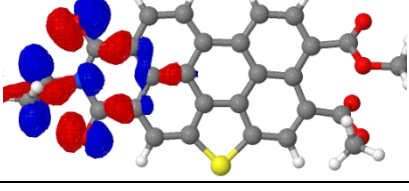
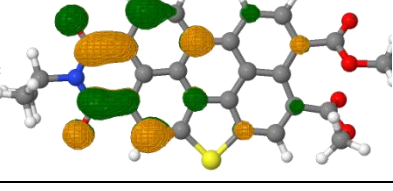
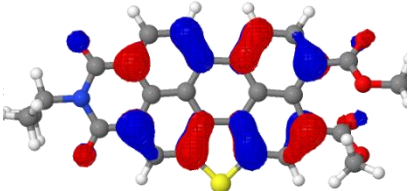
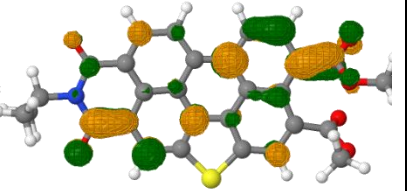
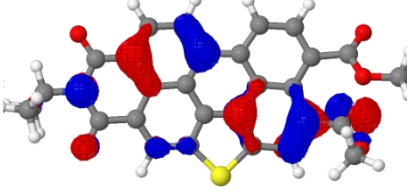
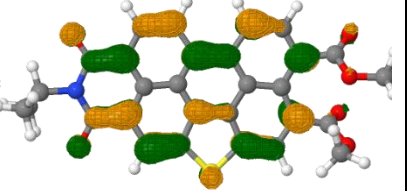
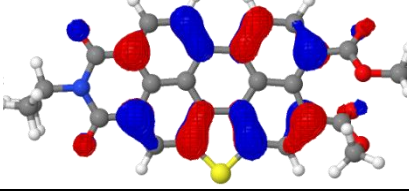
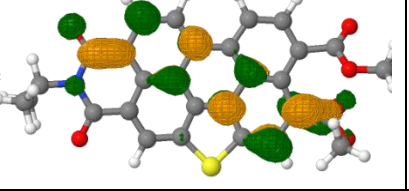
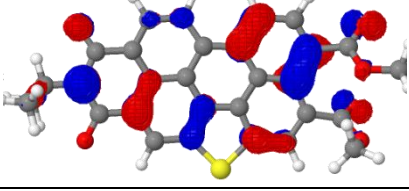
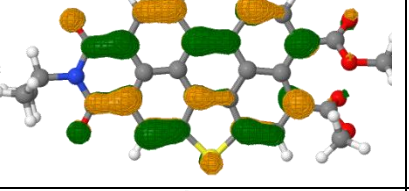
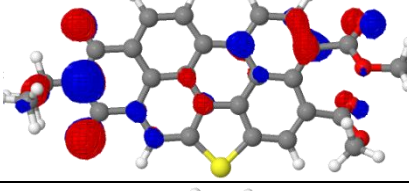
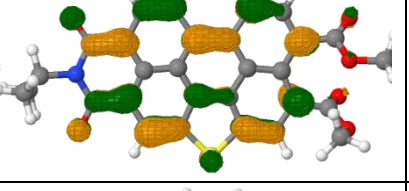
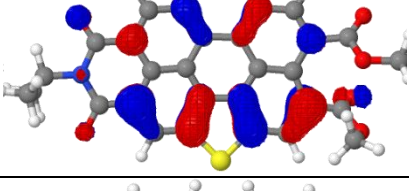
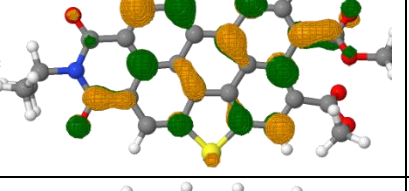
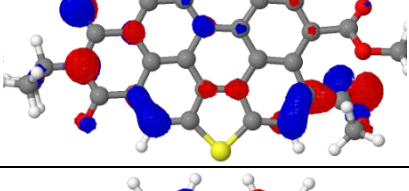
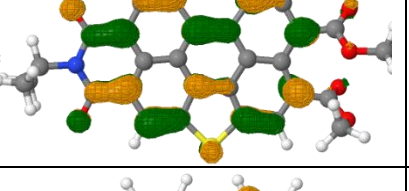
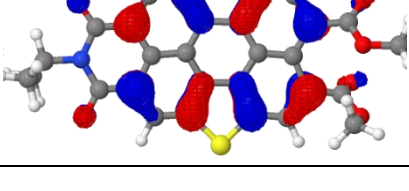
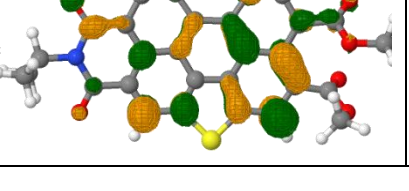


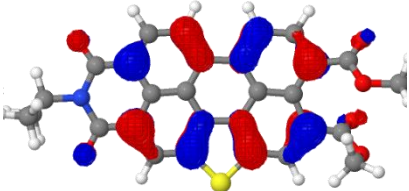
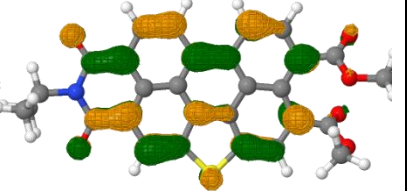
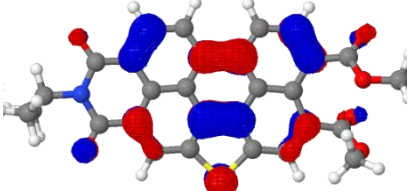
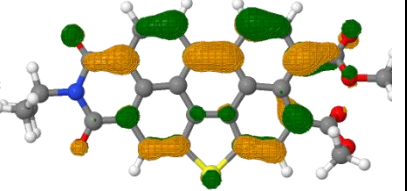
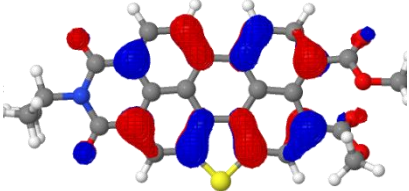
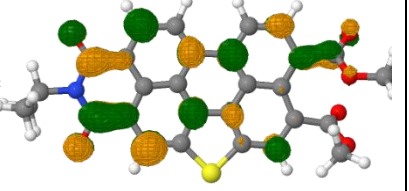
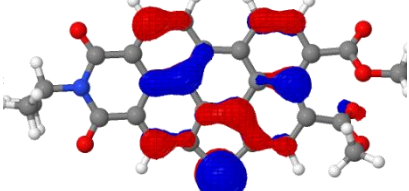
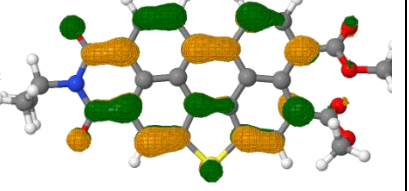
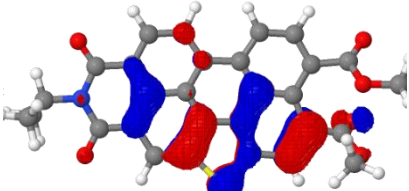
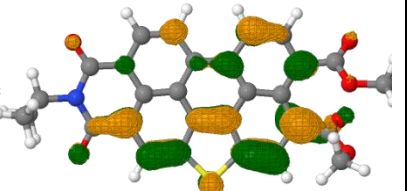
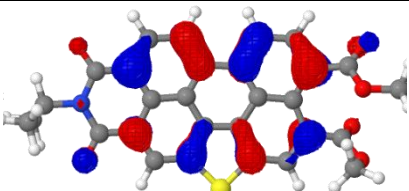
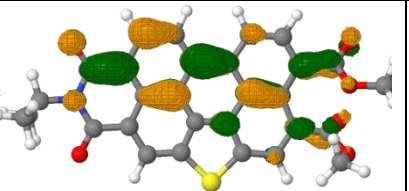
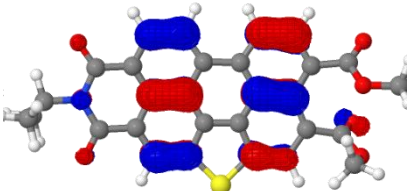
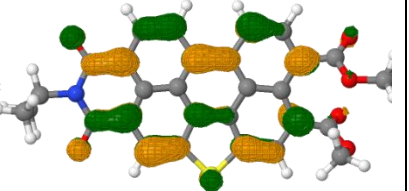
Figure S15. TD-DFT simulated UV-vis absorption spectra of compound **PEI-SST** (no. of states considered =40).

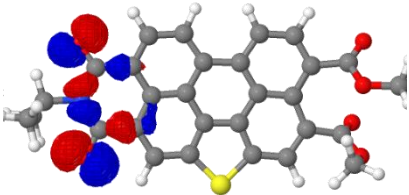
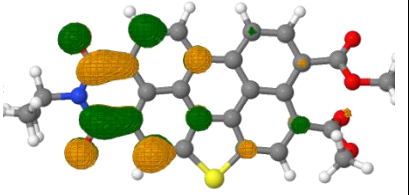
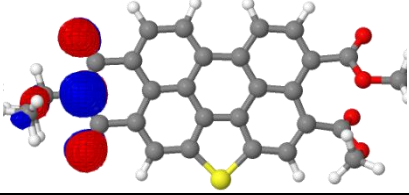
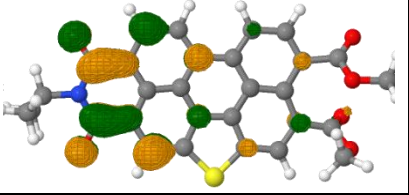
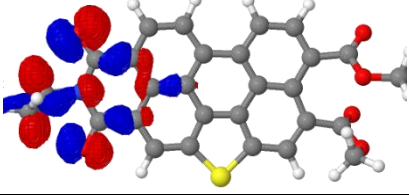
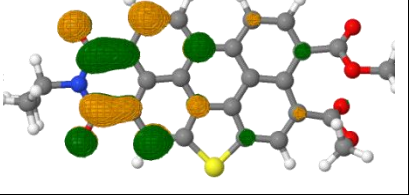
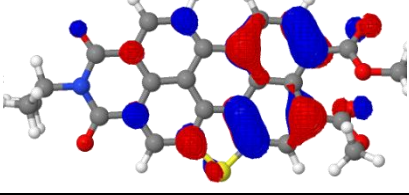
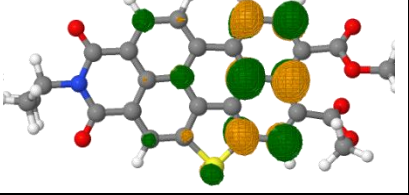
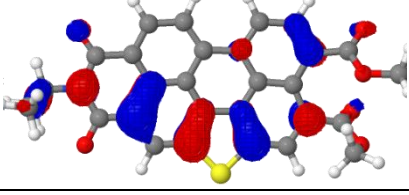
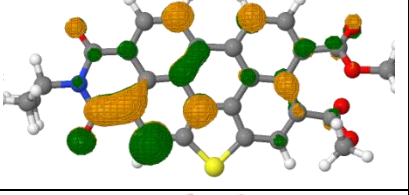
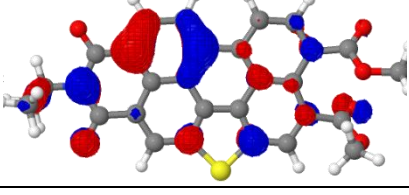
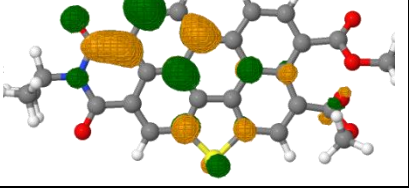
The singlet energy (E_S) of compound **PEI-SST** calculated from the fluorescence spectra (at room temperature) is found to be 2.55 eV (calculated from emission maxima (recorded in CHCl_3 , Fig.S5), while $E_S = 3.102$ eV has been estimated from TD-DFT calculation. No phosphorescence is observed for **PEI-SST**. While from TD-DFT the calculated triplet energy of the T_1 state is $E_T = 1.525$ eV.

Table S6. Calculated natural transition orbitals (NTO) of singlet and triplet excited states.

Excited states (Energies)	Hole	Contribution	Particle	Contribution
S ₁ (3.102 eV)		0.98		0.98
S ₂ (3.657 eV)		0.87		0.87
S ₃ (4.178 eV)		0.92		0.92
S ₄ (4.211 eV)		0.77		0.77
S ₅ (4.268 eV)		0.65		0.65
		0.29		0.29
S ₆ (4.399 eV)		0.88		0.88

S₇ (4.571 eV)		0.58		0.58
		0.37		0.37
S₈ (4.637 eV)		0.53		0.53
		0.41		0.41
S₉ (4.800 eV)		0.63		0.63
		0.30		0.30
S₁₀ (4.896 eV)		0.62		0.62
		0.29		0.29

Triplet states				
Excited states (Energies)	Hole	Contribution	Particle	Contribution
T ₁ (1.525 eV)		0.92		0.92
T ₂ (2.947 eV)		0.51		0.51
		0.37		0.37
T ₃ (2.989 eV)		0.83		0.83
T ₄ (3.098 eV)		0.53		0.53
		0.40		0.40
T ₅ (3.668 eV)		0.73		0.73

T₆ (3.816 eV)		0.88		0.88
T₇ (3.907 eV)		0.77		0.77
T₈ (4.038 eV)		0.83		0.83
T₉ (4.121 eV)		0.81		0.81
T₁₀ (4.136 eV)		0.35		0.35
		0.26		0.26

(a)

Excited States	Hole	Particle
S₁ (3.102 eV)		
T₄ (3.098 eV)		

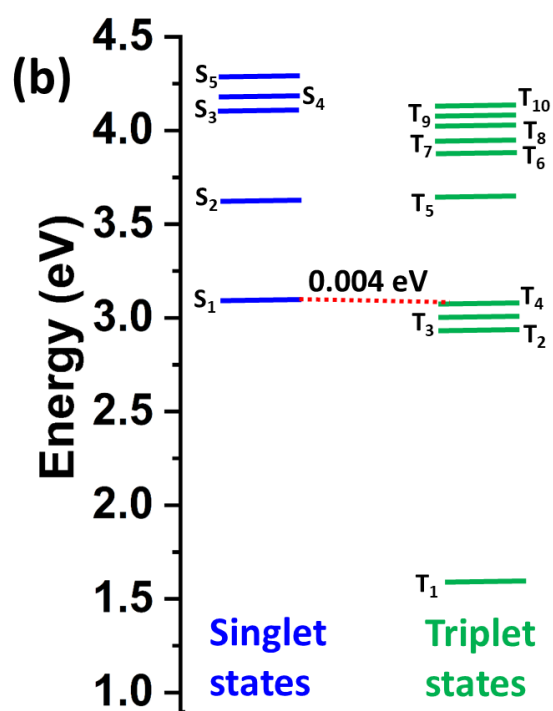


Figure S16. (a) Natural transition orbitals of the S₁ and T₄ excited states for compound **PEI-SST**; (b) Energy level diagram of theoretically calculated singlet and triplet energy states.

15. Electron-hole correlation plots for the individual states

In π -conjugated systems, relying solely on molecular orbitals for descriptions often falls short of providing a comprehensive understanding.^{S14,S15} Instead, a more appropriate approach involves using a coupled electron-hole pair framework, which quantitatively assesses excitonic effects. To gain deeper insights into the excited states, a transition density matrix (TDM) analysis was conducted using the TheoDORE package (Fig. S18-S20).

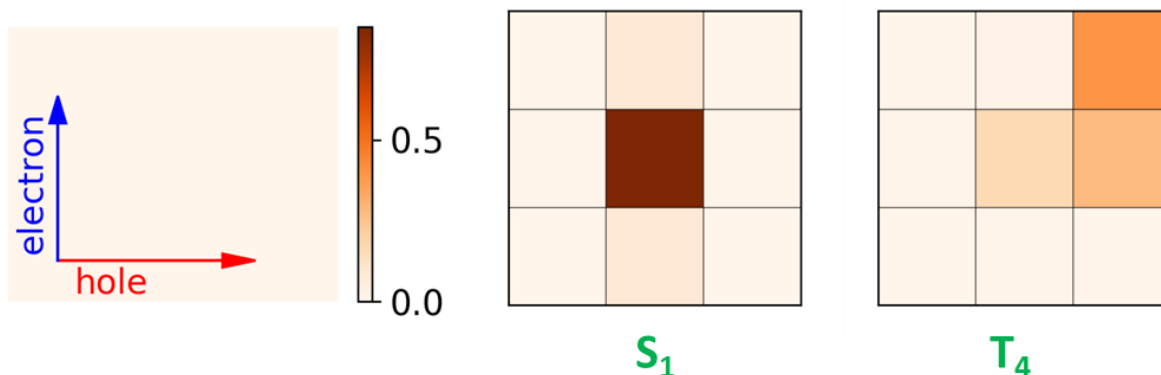


Figure S17. Electron-hole correlation plots of S_1 and T_4 states of compound **PEI-SST**.

The TDM was partitioned into contributions from different fragments, allowing for a detailed examination of the excited state characteristics. Electron-hole correlation plots were further generated for graphical representation. In the plot, the distribution of the excited states across the principal diagonal represents locally excited states, indicating that both electrons and holes are confined within a single unit. The off-diagonal distribution in the matrix indicates the charge transfer character of the excited states. Analyzing the plots shown in Fig. S17-S19, it can be observed that the dark brown zone is localized along the diagonal of the 2D color-filled map. This suggests that the excited states exhibit a dominant Local Excitation (LE) character, with fewer off-white (or light brown) regions in the off-diagonal matrix indicating a weak charge transfer nature. Specifically, for the S_1 and T_4 states, the analysis reveals a dominant LE character with only a substantial amount of charge transfer, further supporting the notion of the electronic transition having a dominant LE character in HLCT process, as mentioned earlier. This finding is consistent with a previous report that evaluated the HLCT nature of the perylene derivative using theoretical investigation.^{S16}

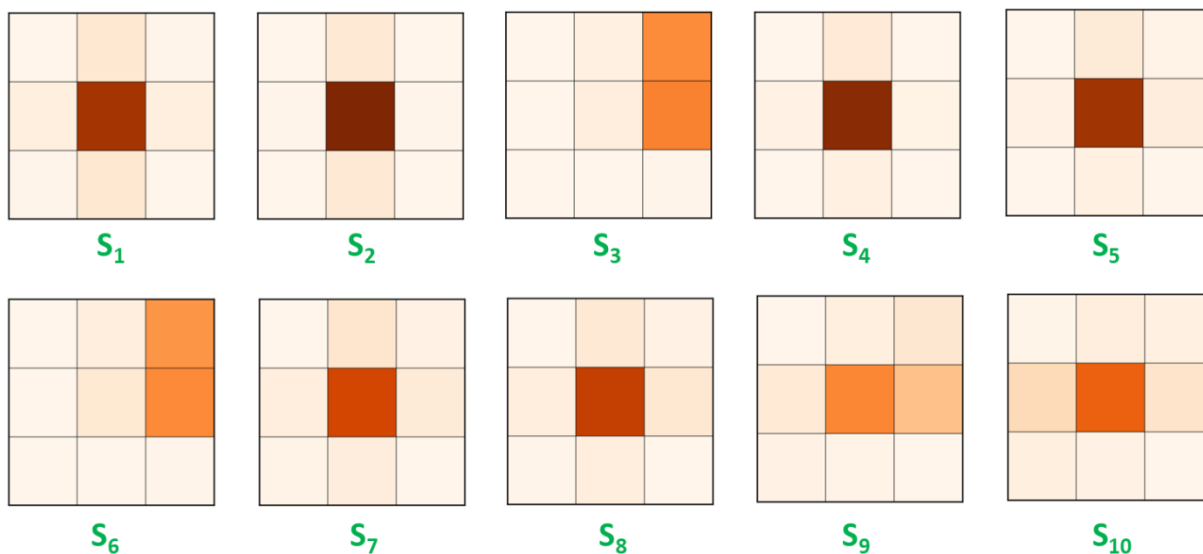


Figure S18. Electron-hole correlation plots of S_1 - S_{10} states of compound **PEI-SST**.

From the above figure it is clear that S_1 , S_2 , S_4 , S_5 , S_7 , S_8 , S_9 , and S_{10} are local excited states with very less charge transfer characteristics while S_3 , S_6 , and S_9 show a dominant charge transfer characteristic.

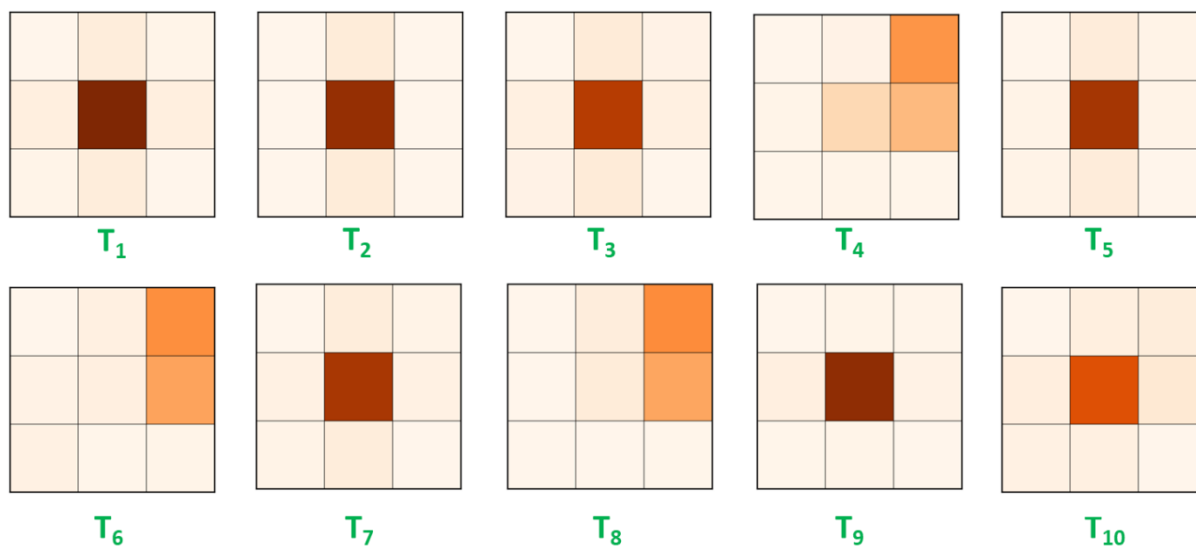


Figure S19. Electron-hole correlation plots of T_1 - T_{10} states of compound **PEI-SST**.

From the above figure, it is clear that T_1 , T_2 , T_3 , T_5 , T_7 , T_9 , and T_{10} are local excited states with very less charge transfer characteristics while T_4 , T_6 , and T_8 show dominant charge transfer characteristics.

16. Time resolved photoluminescence studies

Fluorescence lifetime decay measurements were conducted in chloroform to add to the evidence supporting the HLCT phenomenon in **PEI-SST** (Fig. S20). A single exponential decay with lifespan in the nanosecond time scale was detected in time resolved fluorescence studies of compound **PEI-SST**, demonstrating the lack of a delayed component (TADF) in emission. Although it had a relatively longer lifetime (~ 4.03 ns) than conventional fluorescent emitters, which indicated the presence of hybridized LE and CT components in a single emissive HLCT state,^{S11, S12, S17} which is what caused the EQE in the present case to exceed the upper limit of conventional fluorescent emitters.

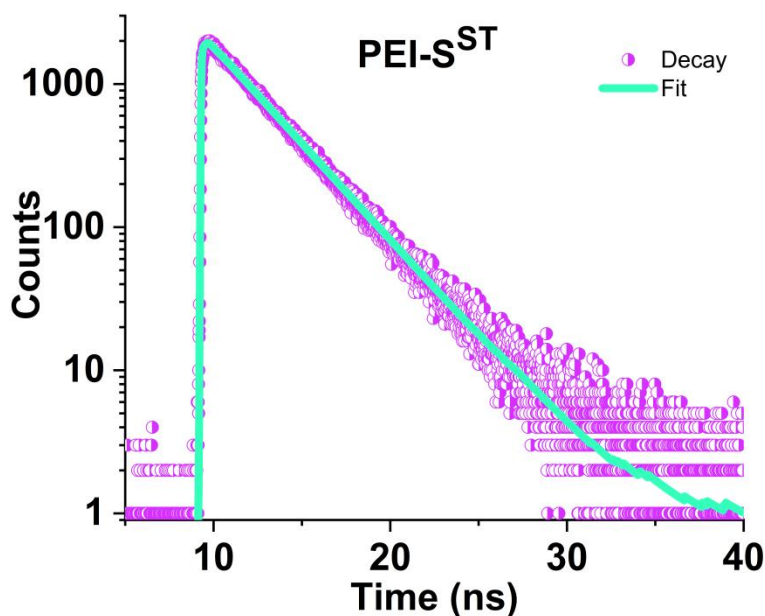


Figure S20. Fluorescence lifetime decay spectra of emitter **PEI-SST** in chloroform; Experimental decay in purple coloured circles; Mono-exponential fit in green coloured line.

17. References

- S1. R. K. Gupta, B. Pradhan, S. K. Pathak, M. Gupta, S. K. Pal, A. A. Sudhakar, *Langmuir*, **2015**, 31, 8092-8100.
- S2. a) Gaussian 09, Revision B.01, M. J. Frisch, G. W. Trucks, H. B. Schlegel, G. E. Scuseria, M. A. Robb, J. R. Cheeseman, G. Scalmani, V. Barone, B. Mennucci, G. A. Petersson, H. Nakatsuji, M. Caricato, X. Li, H. P. Hratchian, A. F. Izmaylov, J. Bloino, G. Zheng, J. L. Sonnenberg, M. Hada, M. Ehara, K. Toyota, R. Fukuda, J. Hasegawa, M. Ishida, T. Nakajima, Y. Honda, O. Kitao, H. Nakai, T. Vreven, J. J. A. Montgomery, J. E. Peralta, F. Ogliaro, M. Bearpark, J. J. Heyd, E. Brothers, K. N. Kudin, V. N. Staroverov, R. Kobayashi, J. Normand, K. Raghavachari, A. Rendell, J. C. Burant, S. S. Iyengar, J. Tomasi, M. Cossi, N. Rega, J. M. Millam, M. Klene, J. E. Knox, J. B. Cross, V. Bakken, C. Adamo, J. Jaramillo, R. Gomperts, R. E. Stratmann, O. Yazyev, A. J. Austin, R.

- Cammi, C. Pomelli, J. W. Ochterski, R. L. Martin, K. Morokuma, V. G. Zakrzewski, G. A. Voth, P. Salvador, J. J. Dannenberg, S. Dapprich, A. D. Daniels, O. Farkas, J. B. Foresman, J. V. Ortiz and J. Cioslowski Fox, *D. J. Gaussian Inc., Wallingford, CT*, **2009**;
- b) C. Lee, W. Yang and R. G. Parr, *Phys. Rev. B*, **1988**, 37, 785–789; c) A. D. Becke, *J. Chem. Phys.*, **1993**, 98, 1372–1377.
- S3. Wong, M.Y. and Zysman-Colman, E., Purely organic thermally activated delayed fluorescence materials for organic light-emitting diodes. *Adv. Mater.*, **2017**, 29(22), 1605444.
- S4. Liu, Y., Li, C., Ren, Z., Yan, S. and Bryce, M.R., All-organic thermally activated delayed fluorescence materials for organic light-emitting diodes. *Nat. Rev. Mater.*, **2018**, 3(4), 1-20.
- S5. Olivier, Y., Moral, M., Muccioli, L. and Sancho-García, J.C., Dynamic nature of excited states of donor–acceptor TADF materials for OLEDs: how theory can reveal structure–property relationships, *J. Mater. Chem. C*, **2017**, 5(23), 5718–5729.
- S6. Luo, Y. and Aziz, H., Correlation between triplet–triplet annihilation and electroluminescence efficiency in doped fluorescent organic light-emitting devices, *Adv. Funct. Mater.*, **2010**, 20(8), 1285–1293.
- S7. Zhang, H., Zeng, J., Luo, W., Wu, H., Zeng, C., Zhang, K., Feng, W., Wang, Z., Zhao, Z. and Tang, B.Z., Synergistic tuning of the optical and electrical performance of AIEgens with a hybridized local and charge-transfer excited state. *J. Mater. Chem. C*, **2019**, 7(21), 6359–6368.
- S8. Wang, C., Li, X., Pan, Y., Zhang, S., Yao, L., Bai, Q., Li, W., Lu, P., Yang, B., Su, S. and Ma, Y., Highly efficient non-doped green organic light-emitting diodes with combination of high photoluminescence and high exciton utilization. *ACS Appl. Mater. Interfaces*, **2016**, 8(5), 3041–3049.
- S9. Zhang, S., Li, W., Yao, L., Pan, Y., Shen, F., Xiao, R., Yang, B. and Ma, Y., Enhanced proportion of radiative excitons in non-doped electro-fluorescence generated from an imidazole derivative with an orthogonal donor–acceptor structure. *Chem. Commun.*, **2013**, 49(96), 11302–11304.
- S10. Hong, W.P. and Tagare, J., Recent Progress in Imidazole Based Efficient near Ultraviolet/Blue Hybridized Local Charge Transfer (HLCT) Characteristics Fluorophores for Organic Light-Emitting Diodes. *J. Mater. Chem. C*, **2022**, 10, 16173-16217.
- S11. Tang, X., Bai, Q., Peng, Q., Gao, Y., Li, J., Liu, Y., Yao, L., Lu, P., Yang, B. and Ma, Y., Efficient deep blue electroluminescence with an external quantum efficiency of 6.8% and CIE $y < 0.08$ based on a phenanthroimidazole–sulfone hybrid donor–acceptor molecule. *Chem. Mater.*, **2015**, 27(20), 7050–7057.
- S12. Konidena, R.K., Thomas, K.J., Dubey, D.K., Sahoo, S. and Jou, J.H., A new molecular design based on hybridized local and charge transfer fluorescence for highly efficient ($> 6\%$) deep-blue organic light emitting diodes. *Chem. Commun.*, **2017**, 53(86), 11802–11805.

- S13. Li, W., Pan, Y., Yao, L., Liu, H., Zhang, S., Wang, C., Shen, F., Lu, P., Yang, B. and Ma, Y., A hybridized local and charge-transfer excited state for highly efficient fluorescent oleds: Molecular design, spectral character, and full exciton utilization, *Adv. Opt. Mater.*, **2014**, 2(9), 892–901.
- S14. Mewes, S.A., Plasser, F. and Dreuw, A., Universal exciton size in organic polymers is determined by nonlocal orbital exchange in time-dependent density functional theory. *J. Chem. Phys.*, **2017**, 8(6), 1205-1210.
- S15. Mewes, S.A., Plasser, F., Krylov, A. and Dreuw, A., 2018. Benchmarking excited-state calculations using exciton properties. *J. Chem. Theory Comput.*, **2018**, 14(2), 710-725.
- S16. Shen, Y., Zhang, Z., Liu, H., Yan, Y., Zhang, S., Yang, B. and Ma, Y., Highly efficient orange-red/red excimer fluorescence from dimeric π - π stacking of perylene and its nanoparticle applications. *J. Phys. Chem. C* **2019**, 123, 13047–13056.
- S17. Shan, T., Liu, Y., Tang, X., Bai, Q., Gao, Y., Gao, Z., Li, J., Deng, J., Yang, B., Lu, P. and Ma, Y., Highly efficient deep blue organic light-emitting diodes based on imidazole: significantly enhanced performance by effective energy transfer with negligible efficiency roll-off. *ACS Appl. Mater. interfaces*, **2016**, 8(42), 28771-28779.